

**AN INSIGHT ON PROCESSING AND CHARACTERIZATION OF IN-SITU
AND IN-SITU HYBRID COMPOSITES WITH LIQUID CRYSTALLINE
POLYMERS**



Penwisa Pisitsak

A Dissertation Submitted in Partial Fulfilment of the Requirements
for the Degree of Doctor of Philosophy
The Petroleum and Petrochemical College, Chulalongkorn University
in Academic Partnership with
The University of Michigan, The University of Oklahoma,
and Case Western Reserve University

2010

530022

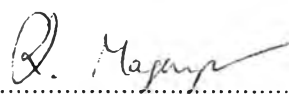
Thesis Title: An insight on processing and characterization of in-situ and in-situ hybrid composites with liquid crystalline polymers
By: Penwisa Pisitsak
Program: Polymer Science
Thesis Advisors: Assoc. Prof. Rathanawan Magaraphan
Prof. Sadhan C. Jana


Accepted by the Petroleum and Petrochemical College, Chulalongkorn University, in partial fulfilment of the requirements for the Degree of Doctor of Philosophy.


..... College Dean
(Asst. Prof. Pomthong Malakul)

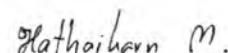
Thesis Committee:



.....
(Asst. Prof. Pomthong Malakul)


.....
(Assoc. Prof. Rathanawan Magaraphan)


.....
(Prof. Sadhan C. Jana)


.....
(Asst. Prof. Manit Nithitanakul)


.....
(Asst. Prof. Hathaikarn Manuspiya)


.....
(Asst. Prof. Chanchai Thongpin)

ABSTRACT

4882001063: Polymer Science Program

Penwisa Pisitsak: An Insight on Processing and Characterization of In-Situ and In-Situ Hybrid Composites with Liquid Crystalline Polymers.

Thesis Advisors: Assoc. Prof. Rathanawan Magaraphan (*Thai Advisor*), Prof. Sadhan C. Jana (*Overseas Co-Adviser*)

Keywords: In-situ composite/ Liquid crystalline polymer/ Multi-walled carbon nanotube/ Zinc oxide

Blends of a liquid crystalline polymer (LCP) and a thermoplastic are generally immiscible. They are termed as 'in-situ composites', taking into account of the formation of LCP fibrils capable of reinforcing the resulting blends. Blends of Vectra A950 (VA950) with poly(trimethylene terephthalate) (PTT) showed better melt processibility as a result of partial LCP fibrillation. The best LCP dispersion was found at the lowest processing temperature and the smallest LCP content. The modulus and thermal stability were improved. VA950 was found to accelerate the non-isothermal crystallization rate of the PTT phase by serving as a nucleating agent. The microwave-synthesized spherical zinc oxide (ZnO) particles were introduced to the blends of VA950 and poly(ethylene terephthalate) (PET). ZnO reduced the LCP fibrillation owing to its lubricating effect, retarded the PET melt crystallization rate, and yet improved the tensile modulus. An increase in the extent of triclinic crystalline phase of PET as induced by microwave radiation was promoted in the presence of VA950, yielding improved mechanical properties. Multi-walled carbon nanotubes (CNTs) were introduced to polycarbonate/ LCP blends where the LCP chosen were VA950 and Vectra V400P (V400P). CNTs showed better affinity with LCP and consequently prohibited LCP fibrillation leading to the disruption of conductive pathways. As a result, a greater CNT loading was required to reach a percolation threshold compared to the composites without LCP. The value of storage modulus showed improvement by the addition of CNTs or VA950.

บทคัดย่อ

เพ็ญวิสาข์ พิสิษฐศักดิ์ : ชื่อหัวข้อวิทยานิพนธ์ (ภาษาไทย) การศึกษากระบวนการขึ้นรูปและวิเคราะห์สมบัติของอินซิทู และ อินซิทู ไฮบริด คอมพอสิต ซึ่งมีส่วนผสมของพอลิเมอร์ผลึกเหลว (An Insight on Processing and Characterization of In-Situ and In-Situ Hybrid Composites with Liquid Crystalline Polymers) อาจารย์ที่ปรึกษา : รศ.ดร. รัตนวรรณ มกรพันธุ์ (อ. คนไทย) และ ศ. ดร. ชัดชาน ชี จานา (อ. ที่ปรึกษาร่วมชาวต่างประเทศ) 206 หน้า

พอลิเมอร์ผสมระหว่างพอลิเมอร์ผลึกเหลว (แอลซีพี) และเทอร์โมพลาสติกโดยทั่วไปเป็นพอลิเมอร์ผสมแบบไม่เข้ากัน พอลิเมอร์ผสมเช่นนี้มักถูกเรียกว่า อินซิทู คอมพอสิต เนื่องจากแอลซีพีที่เปลี่ยนรูปเป็นเส้นใยสามารถช่วยเสริมแรงได้ เมื่อผสมเวคตรา เอ 950 (เวคตราเอ) เข้ากับพอลิไตรเมธิลีน เทเรพทาเลต (พีทีที) พบว่าสมบัติการไหลดีขึ้นเนื่องจากเวคตราเอบางส่วนอยู่ในรูปของเส้นใย การกระจายตัวของเวคตราเอดีที่สุดเมื่อผสมที่อุณหภูมิต่ำและใช้เวคตราเอน้อยที่สุด พบด้วยว่าเวคตราเอทำให้ค่ามอดูลัสและเสถียรภาพทางความร้อนดีขึ้น เวคตราเอยังเป็นตัวเหนี่ยวนำการเกิดผลึกของพีทีที ช่วยให้การตกผลึกแบบอุณหภูมิไม่คงที่ของพีทีทีเกิดเร็วขึ้น ต่อมาได้ทำการศึกษาพอลิเมอร์ผสมระหว่างเวคตราเอ กับ พอลิเอธิลีน เทเรพทาเลต (พีอีที) โดยเติมซิงค์ออกไซด์ในรูปอนุภาคกลมซึ่งสังเคราะห์ขึ้นโดยใช้คลื่นไมโครเวฟ พบว่าซิงค์ออกไซด์ไปลดแรงเสียดทานในการไหลทำให้เส้นใยของเวคตราเอลดลง และยังลดความเร็วในการตกผลึกของพีอีที อย่างไรก็ตามค่ามอดูลัสของคอมพอสิตยังคงเพิ่มขึ้น เมื่อผ่านคลื่นไมโครเวฟ พบว่าในระบบที่ผสมกับเวคตราเอให้ค่าระดับความเป็นผลึกชนิดไตรคลินิกสูงกว่าปกติ เป็นผลให้สมบัติเชิงกลของระบบดีขึ้นด้วย นอกจากนี้ยังได้ทำการศึกษาผลของการเติมท่อนาโนคาร์บอนชนิดผนังหลายชั้นลงในพอลิเมอร์ผสมของพอลิคาร์บอนเนต/แอลซีพี โดยแอลซีพีที่เลือกใช้มีสองเกรดคือ เวคตราเอ และเวคตราวี 400พี พบว่าท่อนาโนคาร์บอนเลือกที่จะอยู่ในแอลซีพี ซึ่งมีผลทำให้เฟสของแอล-ซีพีขาดจากกัน ดังนั้นเส้นทางการนำไฟฟ้าจึงลดลง เป็นผลให้ต้องใช้ปริมาณท่อคาร์บอนเพื่อให้ถึงระดับเพอร์โคเลชันทรานซิสต์มากกว่าระบบที่ไม่ใส่แอลซีพี การผสมเวคตราเอหรือท่อนาโนคาร์บอนส่งผลให้ค่ามอดูลัสสะสมสูงขึ้น

ACKNOWLEDGEMENTS

The author would like to express her sincere gratitude to her adviser Dr. Rathanawan Magaraphan for her intensive suggestions, patience, and encouragement throughout this study.

The author would like to extend her gratitude to Dr. Sadhan C. Jana at The University of Akron (UA) for his guidance and support for partial work in this dissertation.

The author is grateful for the financial support provided by the Thailand Research Fund (TRF-RGJ Program), the Development and Promotion of Science and Technology Talents Project (DPST) scholarship, Polymer Processing and Polymer Nanomaterials Unit, the Asian Development Bank (ADB), The Petroleum and Petrochemical College, and National Center of Excellence for Petroleum, Petrochemicals, and Advanced Materials, Thailand.

Special thanks go to all of The Petroleum and Petrochemical College's faculties who have provided her with invaluable knowledge, and to the College staffs for their helpfulness at every stage of this research.

Also, the author would like to express her appreciation to the PPC friends and her friends in UA for their friendly assistance, cheerfulness, creative suggestions, and encouragement.

Finally, the author would like to dedicate this dissertation to her family for their love, understanding, and support.

TABLE OF CONTENTS

	PAGE
Title Page	i
Abstract (in English)	iii
Abstract (in Thai)	iv
Acknowledgements	v
Table of Contents	vi
List of Tables	x
List of Figures	xiii
Abbreviations	xix
List of Symbols	xx
 CHAPTER	
I INTRODUCTION	1
 II THEORETICAL BACKGROUND AND LITERATURE REVIEW	 4
2.1 Liquid Crystalline Polymer (LCP)	4
2.2 Binary LCP/ thermoplastic blends	5
2.3 In-situ hybrid composites	11
2.4 Double Percolation	19
2.5 Microwave heating of polymers	23
 III EXPERIMENTAL	 25
3.1 Materials	25
3.2 Equipment	25
3.3 Methodology	27

CHAPTER	PAGE	
IV	RHEOLOGICAL, MORPHOLOGICAL, THERMAL, AND MECHANICAL PROPERTIES OF BLENDS OF VECTRA A950 AND POLY(TRIMETHYLENE TEREPHTHALATE): A STUDY ON A HIGH-VISCOSITY RATIO SYSTEM	35
	4.1 Abstract	35
	4.2 Introduction	36
	4.3 Experimental	38
	4.4 Results and Discussion	41
	4.5 Conclusions	50
	4.6 Acknowledgements	51
	4.7 References	51
V	NON ISOTHERMAL CRYSTALLIZATION KINETICS AND MELTING BEHAVIORS OF THERMOPLASTIC/ LIQUID CRYSTALLINE POLYMER BLENDS OF POLY(TRIMETHYLENE TEREPHTHALATE)/ VECTRA A950	74
	5.1 Abstract	74
	5.2 Introduction	74
	5.3 Experimental	75
	5.4 Results and Discussion	77
	5.5 Conclusions	79
	5.6 Acknowledgements	80
	5.7 References	80
VI	INFLUENCES OF A LIQUID CRYSTALLINE POLYMER, VECTRA A950, ON CRYSTALLIZATION KINETICS AND THERMAL STABILITY OF POLY(TRIMETHYLENE TEREPHTHALATE)	89

CHAPTER	PAGE
6.1 Abstract	89
6.2 Introduction	89
6.3 Experimental	90
6.4 Results and Discussion	92
6.5 Conclusions	97
6.6 Acknowledgements	97
6.7 References	97
VII IN-SITU HYBRID COMPOSITES OF POLY(ETHYLENE TEREPHTHALATE)/ LIQUID CRYSTALLINE POLYMER FILLED WITH MICROWAVE-SYNTHESIZED ZINC OXIDE POWDER	111
7.1 Abstract	111
7.2 Introduction	111
7.3 Experimental	114
7.4 Results and Discussion	116
7.5 Conclusions	122
7.6 Acknowledgements	122
7.7 References	122
VIII A STUDY ON ELECTRICALLY CONDUCTIVE BLENDS OF POLYCARBONATE/ LIQUID CRYSTALLINE POLYMER/ MULTI-WALLED CARBON NANOTUBES	140
8.1 Abstract	140
8.2 Introduction	141
8.3 Experimental	142
8.4 Results and Discussion	143
8.5 Conclusions	147
8.6 Acknowledgements	148

CHAPTER		PAGE
	8.7 References	148
IX	STRUCTURAL AND MECHANICAL RESPONSE OF POLY(ETHYLENE TEREPHTHALATE)/ LIQUID CRYSTALLINE POLYMER BLENDS TO MICROWAVE RADIATION	159
	8.1 Abstract	159
	8.2 Introduction	159
	8.3 Experimental	162
	8.4 Results and Discussion	163
	8.5 Conclusions	167
	8.6 Acknowledgements	167
	8.7 References	168
X	CONCLUSIONS AND RECOMMENDATIONS	178
	REFERENCES	181
	APPENDIX	202
	CURRICULUM VITAE	205

LIST OF TABLES

TABLE		PAGE
CHAPTER II		
2.1	Reinforcing modes for thermoplastic polymers	7
2.2	Morphology of dispersed LCP phase (LCP/matrix, 10/90, by weight), related to viscosity ratios of LCP to matrices	7
CHAPTER IV		
4.1	Injection molding conditions for the neat PTT, VA, and their blends	70
4.2	DSC characteristics of VA, PTT, and their blends	71
4.3	TGA results of VA, PTT, and their blends	72
4.4	Mechanical properties of injection-molded PTT and VA10 processed at different temperature profiles	73
CHAPTER V		
5.1	Characteristic data of non-isothermal melt-crystallization exotherms for the neat PTT and PTT/VA blends at various cooling rates	87
5.2	Non-isothermal crystallization kinetic parameters based on the Ozawa method at a temperature of 182°C and cooling rates ranging from 10 to 25°C/min	88
CHAPTER VI		
6.1	Non-isothermal melt-crystallization data for the neat PTT, and PTT/VA blends at various cooling rates	106

TABLE	PAGE
6.2 Non-isothermal melt-crystallization kinetics parameters obtained from the combined Avrami–Ozawa approach at cooling rates ranging from 10 to 25°C/min	108
6.3 Crystallization activation energy of PTT, VA, and their blends	109
6.4 Decomposition temperatures of PTT, VA, and PTT/VA blends at 1% weight loss and residue at 700°C	110
CHAPTER VII	
7.1 Sample designations	135
7.2 Injection molding conditions for the neat PET, VA, and their blends	136
7.3 Thermal characteristics of the samples	137
7.4 Isothermal crystallization data of the samples measured at 200°C	138
7.5 The static mechanical properties of the samples	139
CHAPTER VIII	
8.1 Contact angle determination on polymers	155
8.2 Surface energies (in mJ/m ²) based on the two-liquid geometric method	156
8.3 Summary of interfacial energies calculated from the geometric-mean equation and the harmonic-mean equation	157
8.4 Storage moduli, G' at 40°C, for PC, PC/ LCP blends, and composites with 5 wt% CNT	158
CHAPTER IX	
9.1 The static mechanical properties of PET	176

TABLE	PAGE
9.2 The static mechanical properties of PET /10VA	177

LIST OF FIGURES

FIGURE	PAGE
CHAPTER II	
2.1	Schematic diagram showing molecular order in the LCP 4
2.2	The binary blend of poly(ether imide)/ Rodrun LC-5000 6
2.3	The chemical structure of Vectra A950, a liquid crystal copolyester of 73 mol % p-hydroxybenzoic acid (HBA) and 27 mol % 2-hydroxy-6-napthoic acid (HNA) 9
2.4	The chemical reaction between MA-g-PP and VA. 9
2.5	The wurtzite structure of ZnO 13
2.6	The single-walled structure (a) and multi-walled structure (b) of carbon nanotubes 16
2.7	Schematic illustration of critical volume fraction in the percolative network of spherical inclusions in the random distribution: a) without percolation; b) critical volume fraction percolative network; c) percolative network cluster 17
2.8	DC conductivity σ_{DC} versus nanotube concentration p for composites above the percolation threshold 18
2.9	Volume resistivities of the investigated PC/SAN/CNT composites (stars in circle) and those of the single polymer composites PC-CNT and SAN-CNT 22
2.10	Transmission electron micrographs of the blends prepared by pre-compounding of 2 wt% CNTs in PC, subsequent blending with SAN: (PC-CNT) ₆₀ /SAN ₄₀ , 1.2 wt% CNTs in the blend 22
CHAPTER III	
3.1	Schematic of the 4 point-probe configuration 33

FIGURE	PAGE
CHAPTER IV	
4.1 Rheological curves of PTT, VA and their blends containing various VA contents of 0, 10, 20, 30, 40, 50, 70, and 100 wt% using a 1-mm diameter capillary with an L/D of 20 measured at 280°C, 270°C, 260°C, and 250°C	54
4.2 Plots of compositional dependence of shear viscosity of PTT, VA, and their blends extruded at various temperatures and a shear rate of (a) 400 s ⁻¹ , (b) 800 s ⁻¹ , (c) 1200 s ⁻¹ , and (d) 2000 s ⁻¹	55
4.3 VA/PTT viscosity ratios as a function of shear rate for various temperatures	56
4.4 Plots of ln η_a vs. 1/T for PTT and VA extrudates with VA contents of 0, 10, 20, 30, 40, 50, 70, 100 wt% at a shear rate of 400 s ⁻¹	57
4.5 Plots of compositional dependence of flow activation energy of PTT, VA, and their blends extruded at various shear rates	58
4.6 Scanning electron micrographs of VA/PTT blends showing (a) the fractured surface of the twin-screw extrudate, and (b) the fractured surface of the 20 wt% VA rheometer extrudate after shearing at 2000 s ⁻¹ , 260°C	59
4.7 Scanning electron micrographs of VA/PTT strands extruded through a capillary with a constant strain rate of 2000 s ⁻¹ , temperature 260°C, and VA contents of (a) 10, (b) 20, (c) 30, (d) 40, (e) 50, and (f) 70 wt%	60
4.8 Scanning electron micrographs of residues extracted from the blends of VA/PTT with 10 wt% VA, extruded through a capillary at a shear rate of 2000 s ⁻¹ and temperature of (a) 280°C, (b) 270°C, (c) 260°C, and (d) 250°C	61

FIGURE	PAGE
4.9 Diameter distribution of the VA residue in the rheometer extrudates at a shear rate of 2000 s^{-1} and various temperatures	62
4.10 Scanning electron micrographs of residues extracted from the blends of VA/PTT with a VA content of 10 wt%, extruded through a capillary at temperature 250°C , and shear rate of (a) 400 s^{-1} , and (b) 2000 s^{-1}	63
4.11 DSC second heating traces of the neat VA, PTT, and their blends after melt-annealing at 300°C for 5 min and quenching in liquid N_2 for 10 min. The heating rate is $5^{\circ}\text{C}/\text{min}$	64
4.12 DSC cooling traces of the neat VA, PTT, and their blends. The cooling rate is $10^{\circ}\text{C}/\text{min}$	65
4.13 Scanning electron micrographs of the tensile fractured surfaces of (a) VA10-250, (b) VA10-265, and (c) VA10-280	66
4.14 Elongation at break of injection-molded PTT and PTT/VA blends processed at 250°C	67
4.15 Tensile strength of injection-molded PTT and PTT/VA blends processed at 250°C	68
4.16 Tensile modulus of injection-molded PTT and PTT/VA blends processed at 250°C	69

CHAPTER V

5.1 Non-isothermal melt crystallization exotherms for VA10 at various cooling rates	82
5.2 Plots of $\ln \phi$ versus $\ln t$ for the neat PTT at various relative crystallinities	83

FIGURE	PAGE
5.3 Subsequent melting endotherms of the neat PTT and PTT/VA blends at 10, 30, and 70 wt% VA after non-isothermal melt-crystallization at a cooling rate of 15°C/min	84
5.4 Glass transition temperature (T_g) for the neat PTT and its blend with 10 and 30 wt% VA	85
5.5 Scanning electron micrographs of VA residues of VA10 extrudates from a twin-screw extruder and a capillary rheometer	86

CHAPTER VI

6.1 Non-isothermal melt crystallization exotherms for neat PTT and PTT/VA blends at a cooling rate of 10°C/min	99
6.2 Non-isothermal melt crystallization exotherms for the VA70 blend at five different cooling rates ranging from 10 to 30°C/min	100
6.3 Relative crystallinity function of time of PTT and PTT/VA blends at a cooling rate of 15°C/min	101
6.4 Plots of $\ln \phi$ versus $\ln t$ for neat PTT at various relative crystallinities	102
6.5 Plots of $\ln \phi$ versus $1/T_{cp}$ for neat PTT and their blends at various compositions	103
6.6 TGA thermograms of PTT, VA, and their blends	104
6.7 Scanning electron micrographs of Vectra/PTT strands extruded through a capillary with a constant strain rate of 400 s ⁻¹ , temperature 270°C, and Vectra contents of (a) 10, (b) 30, and (c) 70 wt%	105

FIGURE	PAGE
CHAPTER VII	
7.1 XRD spectra of the synthesized ZnO particles	125
7.2 SEM image of the synthesized ZnO particles	126
7.3 Rheological curves of PET, VA, and their blends with ZnO extruded through a capillary die ($L/D = 20$), at 260°C	127
7.4 SEM images of the capillary rheometer extrudate after extrusion at 260°C , 1600 s^{-1} of (a) PVA, (b) PVA 0.5 ZnO, and (c) PVA 1 ZnO	128
7.5 SEM (left) vs. EDX (right) images of the fractured surface of PVA 1 ZnO (Zn mapping)	129
7.6 SEM (left) vs. EDX (right) images of the PVA 1 ZnO after dissolving the PET phase out (Zn mapping)	130
7.7 DSC heating scans (heating rate of $10^{\circ}\text{C}/\text{min}$)	131
7.8 DSC heating scans performed at $10^{\circ}\text{C}/\text{min}$ on the PET/VA samples after cooling at cooling rates ranging from 2.5 to $30^{\circ}\text{C}/\text{min}$	132
7.9 DSC cooling scans at a cooling rate of 10°C	133
7.10 Isothermal melt crystallization at 200°C	134
CHAPTER VIII	
8.1 Comparison of complex viscosity for PC, PC/ LCP blends, and composites with 5 wt% CNT where the LCP used is V400P (measured at 310°C) (a), and VA950 (measured at 300°C) (b)	150
8.2 SEM micrographs of the LCP residues of PC/V400P injection-molded specimen (a), as-compounded PC/VA950 (b), and PC/VA950 injection-molded specimen (c)	151

FIGURE		PAGE
8.3	SEM micrographs of the LCP residues of the injection-molded specimen of PC/V400P/5wt%CNT (a), PC/VA950/5wt%CNT (b), PC/VA950/5wt% CNT with reversed feeding sequence (c)	152
8.4	TEM micrographs of the thin sections of 5 wt% CNT composites based on the neat PC (a), PC/ V400P (b), and PC/ VA950 (c)	153
8.5	The volume conductivity as a function of CNT concentration	154
CHAPTER IX		
9.1	Sample temperature as a function of time during microwave heating	171
9.2	DSC heating scans of the neat PET samples after various cycles of microwave irradiation	172
9.3	X-ray diffractograms of the PET before and after microwave irradiation at different numbers of cycles	173
9.4	DSC heating scans of the neat PET samples after various cycles of microwave irradiation	174
9.5	X-ray diffractograms of PET/VA blends before and after microwave irradiation at different number of cycles	175

ABBREVIATIONS

CNT	Multi-Walled Carbon Nanotube
DSC	Differential Scanning Calorimetry
EDX	Energy Dispersive X-ray
HBA	p-Hydroxybenzoic Acid
HNA	2-Hydroxy-6-Naphthoic Acid
IV	Intrinsic Viscosity
LCP	Liquid Crystalline Polymer
PC	Polycarbonate
PET	Poly(ethylene terephthalate)
POM	Polyoxymethylene
PTT	Poly(trimethylen terephthalate)
SAN	Poly(styrene-acrylonitrile)
SEM	Scanning Electron Microscopy
TEM	Transmission Electron Microscopy
TGA	Thermogravimetric Analysis
TP	Thermoplastic
V400P	Vectra V400P
VA	Vectra A950
VA950	Vectra A950
WAXD	Wide Angle X-ray Diffraction
XRD	X-Ray Diffractometer
ZnO	Zinc Oxide

LIST OF SYMBOLS

Ca	Capillary Number
η_m	Matrix Viscosity
γ	Shear Rate
τ	Shear Stress
σ	Interfacial Tension
R	Droplet Radius
T	Temperature
$K(T)$	Crystallization Rate Constant
ϕ	Cooling Rate
m	Ozawa Exponent
η_a	Melt Viscosity
E_a	Activation Energy
t	Time
$t_{0.5}$	Half-Time of Crystallization
T_{cp}	Peak Crystallization Temperature
T_{ci}	Initial Crystallization Temperature
T_{cf}	Final Crystallization Temperature
T_g	Glass Transition Temperature
T_m	Melting Temperature
T_{cc}	Cold-Crystallization Temperature
T_c	Melt-Crystallization Temperature
T_d	Decomposition Temperature
ΔH_c	Heat of Crystallization
ΔH_c^*	Normalized Heat of Crystallization
ΔH_m^*	Enthalpy of Fusion
ΔH_m^*	Normalized Enthalpy of Fusion
$C(T)$	Relative Degree of Crystallinity
X	Percent Crystallinity

X_t	Relative Degree of Crystallinity as a Function of Time
$X(T)$	Relative Degree of Crystallinity as a Function of Temperature
n	Avrami Exponent
Z_t	Rate Constant
D	Crystallite Size
λ	X-ray Wavelength
A_0	Constant
B	X-ray Diffraction Broadening
θ_B	Peak Angle
R	Electrical Resistance
ρ	Electrical Resistivity
A	Area
L	Length
σ	Specific Conductivity
λ_{31}	Wetting Coefficient
γ	Interfacial Energy
ω_{12}	Spreading Coefficient
θ	Contact Angle
η^*	Complex Viscosity
G'	Storage Modulus
f	Electric Field Frequency
Q	Dielectric per Unit Volume
ϵ	Relative Permittivity
δ	Loss Angle
ϵ_0	Absolute Permittivity of Free Space
E	Electric Field Strength
R	Universal Gas Constant